

Remote sensing to detect sub-surface peat fires and peat fire scars in the Okavango Delta, Botswana

T. Gumbricht^a, T.S. McCarthy^{b*}, J. McCarthy^a, D. Roy^c, P.E. Frost^d and K. Wessels^d

As a consequence of the constantly shifting water distribution in the Okavango Delta, Botswana, peat accumulated in former wetlands adjacent to receding channels is consumed by fire in successive layers as the peat desiccates. Burning peat has been recorded around the dying Thaoge channel since the mid-19th century. In this study, five different remote sensors were used to detect peat fires in and around the Okavango Delta. ATSR data were used to study the annual cycle from 1999 to 2000, AVHRR data and MODIS data were used to monitor the 2000 fire season, and the MODIS Airborne Simulator and Landsat ETM data were employed for high-resolution studies of single fire events. Peat fires were detected using absolute thresholds in the mid-infrared spectrum, the difference between mid and thermal infrared brightness temperatures, and a threshold in the visible to near-infrared spectrum. Lower thresholds than normally used had to be adopted to detect the fires, which led to an overestimation of fires over other areas. The MODIS Airborne Simulator successfully identified the state of peat fires. Making use of a standard fixed threshold, active-fire detection algorithms, ATSR, AVHRR and MODIS data identified only intense surface fires. Peat fires were distinguished only by using a *priori* knowledge of either spatial distributions or temporal history. Landsat ETM data could not be used to detect these fires. The peat fires have an annual cycle, with a maximum during the dry winter, coinciding with the surface fire season, and a dormant state during the wet summer. Night-time imagery was necessary to detect sub-surface fires. The present area of peat fires in the Okavango is approximately 100 km², which is expected to make negligible contributions to regional trace gas and particulate emissions.

Peat fires play an important role in the functioning of the Okavango Delta ecosystem and are controlled by the shifting distribution of water and hence wetland within the delta.¹ The location of the delta and study area are illustrated in Fig. 1. Early explorers in the 19th century observed peat fires along the lower Thaoge to the north of Lake Ngami. Stigand² described peat fires at the then limits of the Thaoge channel. In recent times, the Thaoge has receded and currently persists for a few tens of kilometres south of its bifurcation point on the Okavango River. The gradual recession of the Thaoge has been accompanied by the burning of the accumulated peat. Peat fires in the Okavango Delta have both natural and anthropogenic causes, primarily lightning and land management, with many ignition sources associated with burning of the surrounding grasslands and of papyrus and reeds in the delta.

The peat in the Okavango accumulates up to a depth of 5 m.¹ It

is formed during the active phase of a distributary channel as organic material accumulates in flanking permanent swamps. Once a distribution channel fails, the peat desiccates from the top down and may be consumed by fire in a series of burns extending over several years, with several scattered burning fronts at different depths. Unlike most surface fires, peat fires evolve relatively slowly and may leave only subtle traces on the surface. The low intensity, continuous smouldering phase typical of sub-surface peat fires results in only limited thermal infrared radiation and no or relatively diffuse smoke plumes, except during the simultaneous burning of associated surface vegetation. Each burn consumes a limited peat layer and may leave a layer of grey ash (Fig. 2). The ash becomes consolidated during the wet season and may support grassland communities. Successive drying of underlying peat results in further burning of deeper peat layers, until the entire peat column is consumed. The complete destruction of a thick profile may take many years.

This study was undertaken to evaluate the potential of identifying peat fires and the scars they leave in savanna environments using different remote-sensing systems; and also to estimate the extent and pattern of annual peat burning in the Okavango Delta.

Monitoring biomass burning using remotely sensed data

The use of remotely sensed data for monitoring biomass burning has a considerable history. Most research has focused, however, on monitoring surface rather than sub-surface fires. Conventional approaches attempt to detect actively burning surface fires using hotspot detection algorithms based on thermal channel data. The timing and spatial extent of burning cannot be estimated reliably from hotspot data, as the sensor may not overpass when burning occurs and because clouds may preclude the detection of active fires.³ Consequently, algorithms that map burnt areas and examine spectral values, rather than relying on hotspot detection, have been developed because the spectral changes induced by surface fires persist for a while. Rather than attempt to review all techniques that map active-fire and burnt areas, we summarize only the different sensing methods used in this study. The main sensing characteristics of these systems, the number of scenes and their acquisition dates are listed in Table 1. In this study, ATSR (Along Track Scanning Radiometer) data were used to investigate the annual peat fire cycle from 1999 to 2000, AVHRR (Advanced Very High Resolution Radiometer) and MODIS (Moderate Resolution Imaging Spectrometer) observations were used to study fire development over the 2000 dry season, and the MODIS Airborne Simulator (MAS) and Landsat ETM (Enhanced Thematic Mapper) results were used for high spatial resolution studies on single dates over the study area.

The MODIS Airborne Simulator is a scanning spectrometer that resembles the MODIS instrument, albeit with 50 bands in the range 0.55–14.3 μm . Unlike the other sensors used in this study, it is mounted on an aircraft rather than a satellite. MAS data were sensed over the Okavango Delta as part of the SAFARI 2000 dry season campaign at a nominal flying height of 20 km

^aDepartment of Land and Water Resources Engineering, Royal Institute of Technology, S-100 44 Stockholm, Sweden.

^bDepartment of Geology, University of the Witwatersrand, Private Bag 3, WITS 2050, South Africa.

^cUniversity of Maryland, Department of Geography and NASA Goddard Space Flight Center, Code 922, Greenbelt, MD 20771, U.S.A.

^dInstitute for Soil, Climate and Water, Private Bag X79, Pretoria 0001, South Africa.

*Author for correspondence. E-mail: mcarthy@geosciences.wits.ac.za

onboard the NASA ER-2 aircraft, with a spatial resolution of approximately 50 m.^{4,5}

The Landsat ETM views the same earth location once every 16 days and lacks a 3.7- μm band useful for active fire detection. Many researchers use Landsat data for mapping burnt areas at high spatial resolution (30 m), using the visible and near-infrared Landsat bands,^{20,21} although Brustet *et al.*²² used Landsat data for active-fire mapping.

The NOAA AVHRR has been widely adopted for fire detection.^{6–8} Most AVHRR fire detection algorithms use the approximately 1.1-km spatial resolution of AVHRR data at nadir.⁹ One of the most common algorithms for AVHRR active fire detection is described by the following threshold formula, which is based on the physical principle that radiances observed at shorter wavelengths increase more rapidly than at longer wavelengths as the fire temperature increases:

$$\text{MIR} \geq C_1, \text{MIR} \geq \text{TIR} + C_2 \text{ and } \text{TIR} > 250 \text{ K} \quad (1)$$

where C_1 and C_2 are constants used to describe the threshold of the AVHRR's 3.7- μm middle infrared (MIR) and the 10.8- μm thermal infrared (TIR) bands. Early studies used an MIR threshold (C_1) of approximately 320 K, followed later by the use of a threshold difference between the MIR and TIR (C_2) of approximately 15 K. The TIR threshold of 250 K was introduced to reduce false signals caused by clouds. Many researchers have modified this algorithm for regional application. For example, Kennedy *et al.*¹⁰ introduced a top-of-the-atmosphere reflectance threshold of the near-infrared (NIR) channel (e.g., $\rho_2 \leq 16\%$) to discriminate highly reflective soil surfaces in West Africa. Similarly, AVHRR algorithms have been developed to process night-time data.¹¹

Flasse and Ceccato,¹² amongst others, introduced contextual methods where fixed thresholds are used to identify potential fires and to eliminate cloud pixels, after which neighbouring pixel values are considered to confirm fire presence in an adaptive manner. In a recent evaluation of AVHRR fire detection algorithms, Giglio *et al.*⁹ found the thresholds generally adopted for the 3.7- μm band (316–320 K) to be conservative. They suggested thresholds of 310 to 314 K in the 3.7- μm band (308 K for night-time application), with a 3.7–10.8- μm difference threshold of 7 K (3 K at night) and $\rho_1 \leq 25\%$ using a contextual algorithm.

Single-date AVHRR data have been used to map burned areas over small regions by manual interpretation or by application of thresholds and classification techniques to individual AVHRR bands and derived spectral vegetation indices.¹³ Automated algorithms that map burned areas using multi-temporal AVHRR data under change detection schemes have received considerable attention.^{14,15} These methods examine the magnitude and direction of temporal changes in spectral vegetation indices and surface temperature estimates in order to differentiate between dynamic changes associated with burning from static features that may be spectrally similar to burned areas (for example,

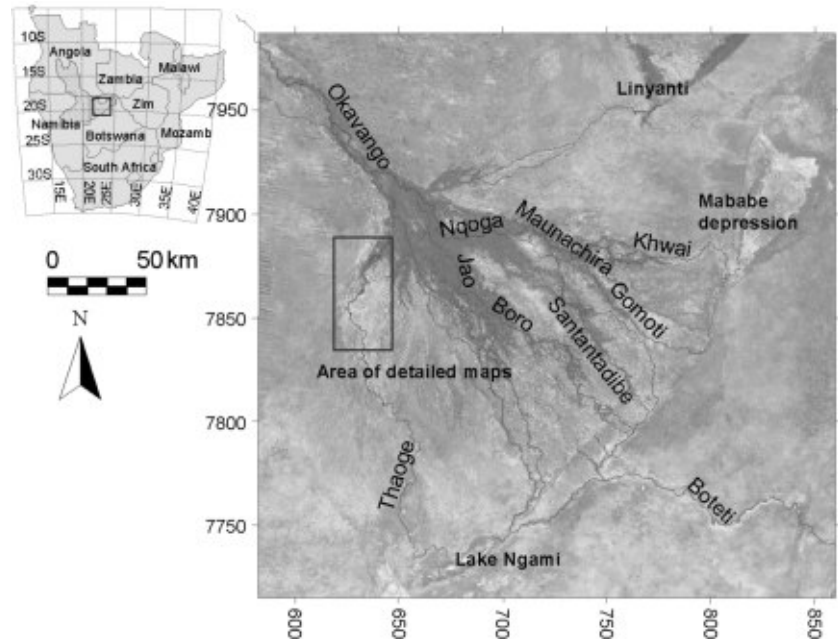


Fig. 1. Study areas within the Okavango Delta, Botswana. The maps are projected to S UTM 34, using the Cape datum (central meridian: 21; scale factor: 0.9996; false easting: 500 000; false northing: 10 000 000). The coordinates are given in kilometres on the main map. The frame marks the area extent of Figs 7 and 9.



Fig. 2. Active peat fire in the Okavango Delta.

water bodies and urban areas). However, they are highly sensitive to the consistency and reliability of pre-processing the AVHRR data.

The ATSR instrument on the ERS satellites has a similar spatial resolution to the AVHRR and benefits from improved geometric characterization and radiometric calibration. The ATSR sensor does not have a near-daily equatorial revisit cycle and typically observed the same point on the equator once every nine days. However, this low revisit period is expected to be less of a limitation for monitoring slowly evolving peat fires. Fixed threshold active-fire detection algorithms have been applied to ATSR data with a global active-fire product defined by thresholding the night-time 3.7- μm data.¹⁶ A study of burned-area mapping was recently undertaken in central Africa¹⁷ by considering temporal changes in the estimates of the ATSR 1.6- μm and land surface temperatures.

Table 1. Sensors and scenes used in this study to detect peat fires in the Okavango Delta.

Sensor/scenes	AVHRR ⁱ	ATSR ⁱⁱ	MODIS ⁱⁱⁱ	MAS ^{iv}	ETM ^v
Approximate spatial resolution at nadir (m)	1100	1000	15, 30, 60	250, 500, 1000	50
No. of bands	5	7	8	36	50
Approximate equatorial revisit period (days)	2	9	16	2	N/A
Centre mid-IR wavelength (µm)	3.7	3.7	2.2	3.9	3.9
Centre thermal IR wavelength (µm)	10.8	10.8	11.45	11.0	11.0
Centre visible-NIR wavelength (µm)	0.9	0.67	0.66	–	0.75
No. of scenes	30	12	3	25	1
Acquisition date(s)	12 Aug – 19 Oct 2000	1999 and 2000 fire seasons	30 Aug 1999 3 Apr 2000 10 Apr 2000	21 Aug – 14 Sep 2000	27 Aug 2000

ⁱAdvanced Very High Resolution Radiometer. ⁱⁱAlong Track Scanning Radiometer. ⁱⁱⁱModerate Resolution Imaging Spectroradiometer. ^{iv}MODIS Airborne Simulator. ^vEnhanced Thematic Mapper.

A global 1-km daily active product is being produced systematically by the U.S. space agency NASA based on a heritage contextual AVHRR algorithm optimized for the MODIS sensor.¹⁸ A 500-m experimental burned-area product is being created for southern Africa using a multi-temporal change detection algorithm³ and using the MODIS daily 500-m land surface reflectance at 1.24 µm, 1.64 µm and 2.13 µm.¹⁹ The MODIS instrument calibration and land products were still being refined during the 2000 dry season study period and so the MODIS results described in this paper are provisional.

Data and methods

We used different algorithms to identify biomass burning, and specifically peat burning, in the Okavango study area with the five different sensors (Table 1). Both active-fire detection and burned-area mapping algorithms were examined. The slow evolution of peat fires implies that the timing of remotely sensed data acquisition is less critical than that required to record surface fire activity. Consequently, this study used remotely sensed data acquired at different times of the day and in different months and years. Great effort was made to acquire cloud-free data.

NOAA AVHRR

In total, 30 NOAA AVHRR scenes covering the period from 12 August to 19 October 2000 were calibrated geometrically and radiometrically. Geometric corrections were applied using both orbital and ground control points, the latter generated using cross-correlation techniques. Radiometric corrections on the visible and near-infrared channels were performed using the post-launch calibration formulae of Rao and Chen.²³ The formulae were derived by calculation of the top-of-the-atmosphere albedo for a 10-year period at calibration sites in the south-eastern Libyan Desert.

The corrected AVHRR scenes were used for fire detection using:

$$MIR \geq C_1, MIR \geq TIR + C_2, TIR > 250 K, \rho_2 \leq C_3\%$$

where MIR and TIR are the brightness temperatures of the 3.7-µm and 10.8-µm bands, and ρ_2 is the top-of-the-atmosphere reflectance of the 0.9-µm near-infrared band. For each scene fire brightness temperatures were extracted for two peat fires, and one peat-related surface fire on 27 August, and one conventional surface fire on 23 August. The constants C_1 , C_2 and C_3 were then individually adjusted for each scene at two levels, accounting for intense (more certain) and low-grade fires, respectively. The adjustment was done using a false-colour composite (red = band 3, green = band 2 and blue = band 1) as a backdrop. Thresholds were set so that the peat fires were detected, irrespective of other (erroneous) detections.

ATSR

Twelve ATSR night-time and daytime scenes were analysed during the 1999 and 2000 fire seasons. For both the wet and dry season images, the daytime 12.0-µm thermal band became saturated for most of the scenes (except for water-inundated areas), and for the dry season also the 10.8-µm band became saturated. To identify fires manually in the daytime ATSR scenes, the 0.67-µm, 3.7-µm and 10.8-µm bands were displayed as blue, green and red. For the night-time ATSR scenes, the 3.7-µm, 10.8-µm and 12.0-µm bands were used. For both night and day scenes, Equation (1) was applied to active peat fire detection by substituting MIR for the 3.7-µm band and TIR for the 10.8-µm band, and the 0.67-µm band for ρ_2 (daytime only).

Landsat ETM

Three geometrically and radiometrically calibrated Landsat ETM 7 scenes were used to map burned areas (175/073 on 30 August 1999 and 10 April 2000; 174/073 on 3 April 2000). Land surface temperatures were calculated for each scene by converting the 60-m 11.45-µm thermal band to black body temperature.²⁴ The black body temperature was adjusted to surface temperature by multiplying by emissivity (ϵ) derived from the natural logarithm of the normalized difference vegetation index (NDVI) as suggested by van de Griend and Owe²⁵ for savanna environments in Botswana:

$$\epsilon_0 = 1.0094 + 0.047 \times \ln(\text{NDVI}), \tag{2}$$

where NDVI was calculated as (NIR – red)/(NIR + red) from the same Landsat TM scene as the derived black body temperature.

The panchromatic ETM band at 15-m resolution was used as a substitute for albedo. The derived NDVI, temperature and albedo were combined, and threshold formulae searching for areas of high temperature and albedo, and low NDVI were used to locate burned areas. The general fire detection formula Equation (1) was also applied to the Landsat ETM data, substituting MIR for the 2.2-µm band and TIR for the 11.45-µm band, and ρ_2 for the 0.66-µm band. Constants C_1 , C_2 and C_3 were adjusted by iteration.

Scene 175/073 (acquired 30 August 1999) was also used to detect scars of peat fires, using both supervised and unsupervised classification. Training and evaluation data were collected in areas with known active peat fires and peat fire scars.

MODIS

Twenty-five days of MODIS daily 500-m land surface reflectance data¹⁹ and daily 1-km active fire products¹⁸ were used to apply the experimental MODIS burned-area algorithm³ and to verify the algorithm, respectively. These data were acquired in the period from 21 August to 14 September 2000. During this

Table 2. Areas corresponding to peat fires and peat fire scars in the Okavango Delta.

Date	Sensor:	ATSR		AVHRR	MAS	
		Peat fire (km ²)		Peat fire (km ²)	Peat fire (km ²)	Peat fire scar (km ²)
30 Aug 1999		6 (day)	–	–	–	–
2 Sep 1999		55 (night)	–	–	–	–
5 Sep 1999		14 (night)	–	–	–	–
7 Oct 1999		3 (day)	–	–	–	–
18 Apr 2000		1 (night)	–	–	–	–
12 Aug 2000		–	13	–	–	–
27 Aug 2000		–	–	54	200	–
28 Aug 2000		–	60	–	–	–
31 Aug 2000		–	81	–	–	–
24 Sep 2000		–	49	–	–	–
3 Oct 2000		–	45	–	–	–
3 Dec 2000		–	38	–	–	–

time, the active-fire detection algorithm was known to be under-performing, the MODIS calibration was being refined, and the MODIS cloud mask algorithm was known to be falsely labelling certain fires and desert regions as cloud.³ The MODIS 1-km day and night active-fire products were temporally combined for comparison with the results of the 500-m experimental MODIS burned-area algorithm, which maps both the location and approximate day of burning.

MODIS Airborne Simulator

The MAS sensed the Okavango Delta in several overpasses on 27 August 2000. For this study only the raw data, without calibration or geometrical information, were available. Only the overpass covering the western part of the delta, with known peat fires around Thaoge, was used in the study. The MAS data were geocorrected using 80 ground control points derived from comparisons with the geolocated Landsat ETM data. Active-fire areas in the MAS data were visually identified (Fig. 7). Two apparent large fires including a fire front, an area with bare soil, and a vegetated surface were analysed for their radiometric properties. As the scene was uncalibrated, all radiometric signals were normalized against the signal of the darkest pixels (water surface) in the scene. Intense and low-grade fires were then identified by adopting Equation (1), with constants iteratively adjusted for a best fit with the temperature profiles. We used the 3.9- μm , 11.0- μm , and the 0.75- μm MAS bands as a visible-NIR channel for distinguishing hot bare soil.

The MAS data were also used to detect old peat fire sites from burn scars. This was done by comparing the spectral signal in regions with known scars with signals from bare soil surfaces and grasslands outside the scar regions.

Results and discussion

The areas corresponding to peat fires varied greatly between sensors, date and time of data acquisition (Table 2). For the

AVHRR sensor, threshold temperatures in the MIR region (3.7 μm) had to be set at 300 K in the early fire season, and approached 310 K later in the season. The ATSR sensor was defaulted at 309 K for daytime images and at 285 K for night-time scenes. The MIR-TIR difference threshold was set at approximately 3 K. These lower than normal thresholds led to an over-estimation of surface fire areas, especially late in the fire season. Surface fire scars often lack vegetation, and because of the ash present, have a lower brightness in the visible to NIR region than bare ground. By contrast, such areas have a higher brightness in the thermal infrared region. As temperatures rise during the dry season (towards summer), both AVHRR and ATSR data tend to become saturated in the thermal bands. To separate peat fires from surface fires, *a priori* knowledge about land cover, juxtaposition or long-term (that is, several months) fire history needs to be included.

The development of fires during the 2000 fire season (August to October) was illustrated using a series of AVHRR scenes, which showed an intense burning from late August onwards (Fig. 3). Peat fires could be distinguished from surface fires by their recurrence sometimes over several months. The peat fires had an elevated brightness temperature during the whole fire season (Figs 3, 4), but also the surface fire scars showed a long period of increased brightness temperature. Most surface fires had a distinctive beginning with saturation (322.5 K) in the 3.7- μm band, and the two more distinct peat fires each had a surficial phase (Fig. 4).

The state of peat fires from 1999 to 2000 was analysed by using a series of ATSR scenes (Fig. 5). The AVHRR and ATSR scenes revealed that one of the peat fires persisted almost unchanged in area from the 1999 to the 2000 fire seasons, albeit with a dormant phase during the (wet) summer. The other peat fires around the dying Thaoge channel were also of long duration (Fig. 5), although not over two seasons. The ATSR sensor was better able to discriminate peat fires (especially from night-time images).

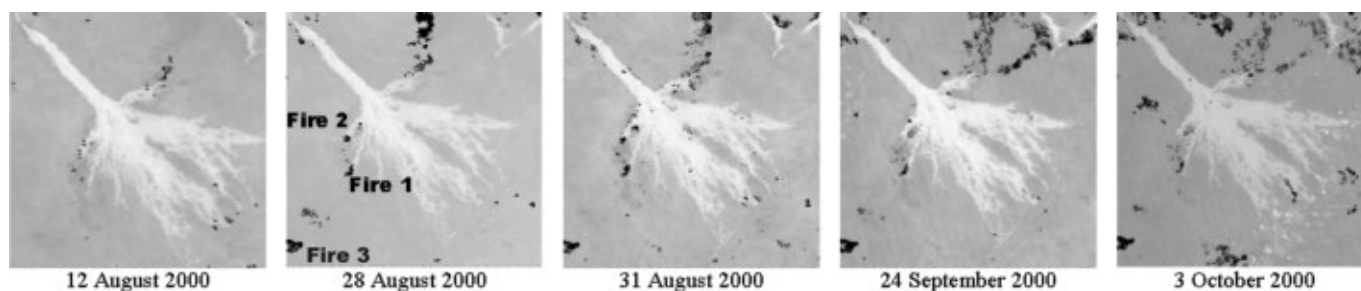


Fig. 3. Fires (dark spots) in the Okavango Delta during the 2000 fire season, detected using AVHRR data. Image backdrop from the AVHRR 3.7- μm band. Fires 1 and 2 are peat fires, Fire 3 is a surface fire.

Figures 6(a) and 6(b) show the MODIS 1.24- μm 500 m land surface reflectance data sensed over the Okavango on 21 August and 14 September 2000. The MODIS 1.24- μm band is shown because it is largely insensitive to smoke aerosols²⁶ and is relatively efficient at distinguishing burnt from unburnt areas in southern Africa.³ The MODIS 500-m data have a considerably higher apparent spatial resolution than the 1-km AVHRR data shown in Fig. 3. The linear features to the west and north of the delta (light tones) are relict sand dunes. These features should not be confused with the faint stripes occurring every 10 km, which were caused by a calibration artefact. The progressions of several extensive burns (dark tones) are clearly evident in these two images.

Figures 6(c) and 6(d) show the results of the MODIS active-fire algorithm¹⁸ and the MODIS burned-area algorithm³ applied to the 25 days of MODIS data sensed over the period spanning the dates illustrated in Figs 6(a) and 6(b). Figure 6(c) shows a temporal composite of the MODIS 1-km day and night active-fire products, and Fig. 6(d) illustrates the 500-m burnt area results for the 25-day period. Both images are shaded to indicate the day of burning. The spatio-temporal progression of burning is clearly evident in these figures, with the majority of the detected active-fire pixels and the regions between them labelled as burnt. The MODIS active-fire algorithm identified the same peat fire areas as were detected with the MAS and AVHRR. The total area of peat burning over the 25-day period was approximately 155 km². The two main peat fire areas identified (Fires 1 and 2 in Fig. 6(d)) had areas of approximately 55 and 60 km².

The high spectral and spatial resolution of the MAS data allowed detection of the peat fires and an associated grassland surface fire front (Fig. 7). The spectral properties of the fire front, the peat fires, a hot soil surface, and a vegetated surface as registered in MAS are shown in Fig. 8. The areas detected as fires in the MAS data, together with the corresponding areas recorded by the AVHRR for the same period, are shown in Fig. 9. One of the peat fires in Fig. 7 (Fire 2) can already be seen in the ATSR data as a peat fire site in September 1999 (Fig. 5). The other fire area (Fire 1) was more persistent than any surface fire registered by the AVHRR data. The more intense Fire 1 had a stronger radiometric signal than Fire 2 (Fig. 8). We interpret Fire 2 as being a combined burning of regrown grassland on an old peat fire area, probably with a fairly thick accumulated ash layer. Fire 2 is less clearly identified in the more coarse-grained data from the

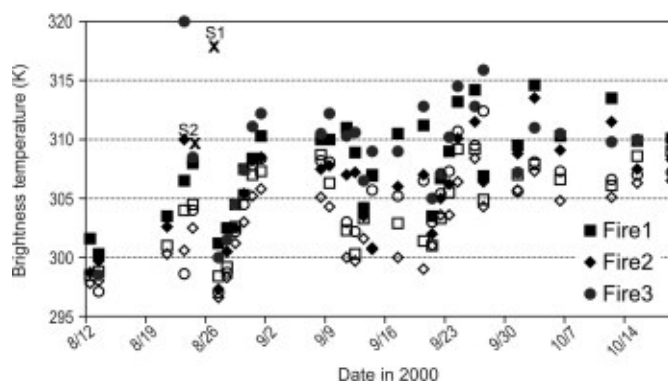


Fig. 4. Brightness temperature of peat fires (Fires 1 and 2 in Fig. 3) and surface fire (Fire 3 in Fig. 3), as recorded by the AVHRR sensor during the 2000 fire season. Filled markers are for MIR (3.7- μm band) and unfilled for TIR (10.9- μm band). The surface fire burned on August 23, after which the signal corresponds to the burn scar. The peat fires each had a surficial phase with elevated brightness temperatures; Fire 1 on 27 August (marked S1) and Fire 2 on 24 August (marked S2). Variations are largely dependent on partial cloud cover and smoke plumes from adjacent fires. Missing data are due to cloud cover. The burn scar from the surface fire remained warmer than the peat fires for approximately one month.

2000 fire season. It is clearly seen, however, in the ATSR night-time image acquired at the beginning of the 1999 fire season (Fig. 5). The most active peat fires occurred on the fringes of the wetland area of the Thaoge channel. We speculate that the peat fires in those regions readily ignited grass that became established during the wet seasons.

The MAS data were also used to identify scars from older peat burns far down the Thaoge channel (Fig. 9a). Indeed, the scars left from peat fires were detectable after several decades. The peat fire scar area around the old Thaoge channel detected with the MAS data was approximately 200 km², which we consider is a minimum extent of peat fires over the last half century. From rule-based, multisource studies on land cover (McCarthy and Gumbricht, in prep.), we estimate the total peat fire burn area around the Thaoge since the beginning of its desiccation about 150 years ago to be 700–1000 km², based on flooding frequency, Landsat TM spectral reflectance and landscape juxtaposition.

The fires could not be uniquely identified in the Landsat ETM data. The lack of a suitable band in the 4 μm region forced the use of a shorter wavelength for fire detection. As seen in Fig. 8, this is not possible for hot environments like the Kalahari. Nor could

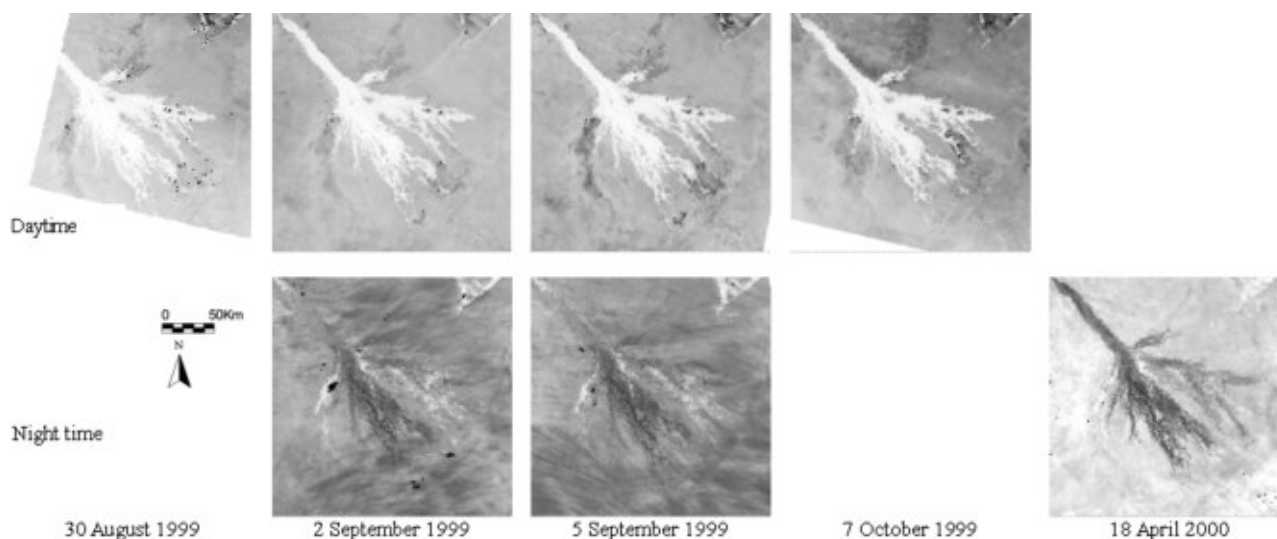
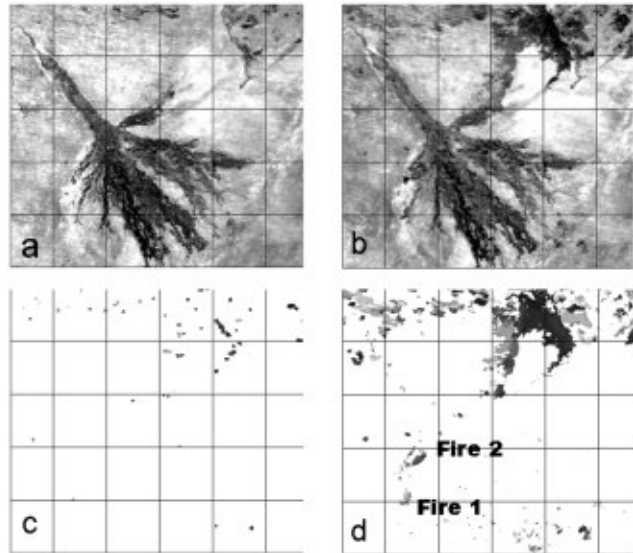


Fig. 5. Fires (dark spots) in the Okavango Delta during the 1999 fire season and the following wet season, detected using ATSR data. Image backdrop from the ATSR 3.7- μm band.

Fig. 6. (a) MODIS 500-m, 1.24- μm land surface reflectance data acquired on 21 August 2000; (b) MODIS-500 m, 1.24 μm land surface reflectance data acquired on 14 September 2000; (c) temporal composite of the MODIS 1-km day and night active-fire products for the period 21 August to 14 September 2000 (shaded with a chronological grey scale: black = beginning of the 25-day period, light grey = end of the period, white = no active fire detected at time of satellite overpass); (d) 500-m MODIS burnt-area results showing the date and location of burning that occurred between 21 August and 14 September 2000 (shaded with a chronological grey scale: black = beginning of the 25-day period, light grey = end of the period, white = no burns detected). The gridlines are spaced at 50-km intervals.



we identify the fires from temperature, albedo or vegetation index data derived from the ETM data. We also could not identify the peat burn scars using traditional supervised or unsupervised classification.

Conclusion

The best sensor for detecting fires in this study was the MODIS Airborne Simulator. The MAS data could detect a regular peat fire and a probable combined grassland-peat fire, including a fire front. The surficial phases of the peat fires were also identified with AVHRR and MODIS observations. One of the peat fires clearly lasted from 1999 to the 2000 fire season. Identification of the peat fire with the AVHRR data led to an overestimation of fire area in the region, especially late in the hot fire season. The ATSR data revealed that the peat fire was dormant during the wet season, which was confirmed by late burning season AVHRR data (not shown). The AVHRR, MODIS and MAS results revealed that the peat fires occasionally turned into flaming surface fires of short duration.

We conclude that peat burning in the desiccating parts of the Okavango Delta has an annual cycle, with high intensity during the dry winter and low intensity during the wet summer. Closer to the front of the receding waters, the peat burns constantly, whereas the fires become intermittent as the front grows further away. The most active peat fires today occur on the fringes of the present wetland area of the Thaoge channel. The area of peat fires is between 75 and 150 km². The peat fire scar area around the old Thaoge channel detected with the MAS data was approximately 200 km². We estimate the total peat fire area around the Thaoge to have been 700–1000 km² over the last 150 years.

Detection of peat fires from space-borne platforms in hot dry environments like savannas or semi-deserts demands a higher degree of manual interpretation than does identification of surface fires. Peat fires have a lower brightness temperature, generate no smoke and only subtle scars. The best option for detecting peat fires with single-scene, low-resolution sensors is to use mid to thermal infrared data acquired at night. AVHRR

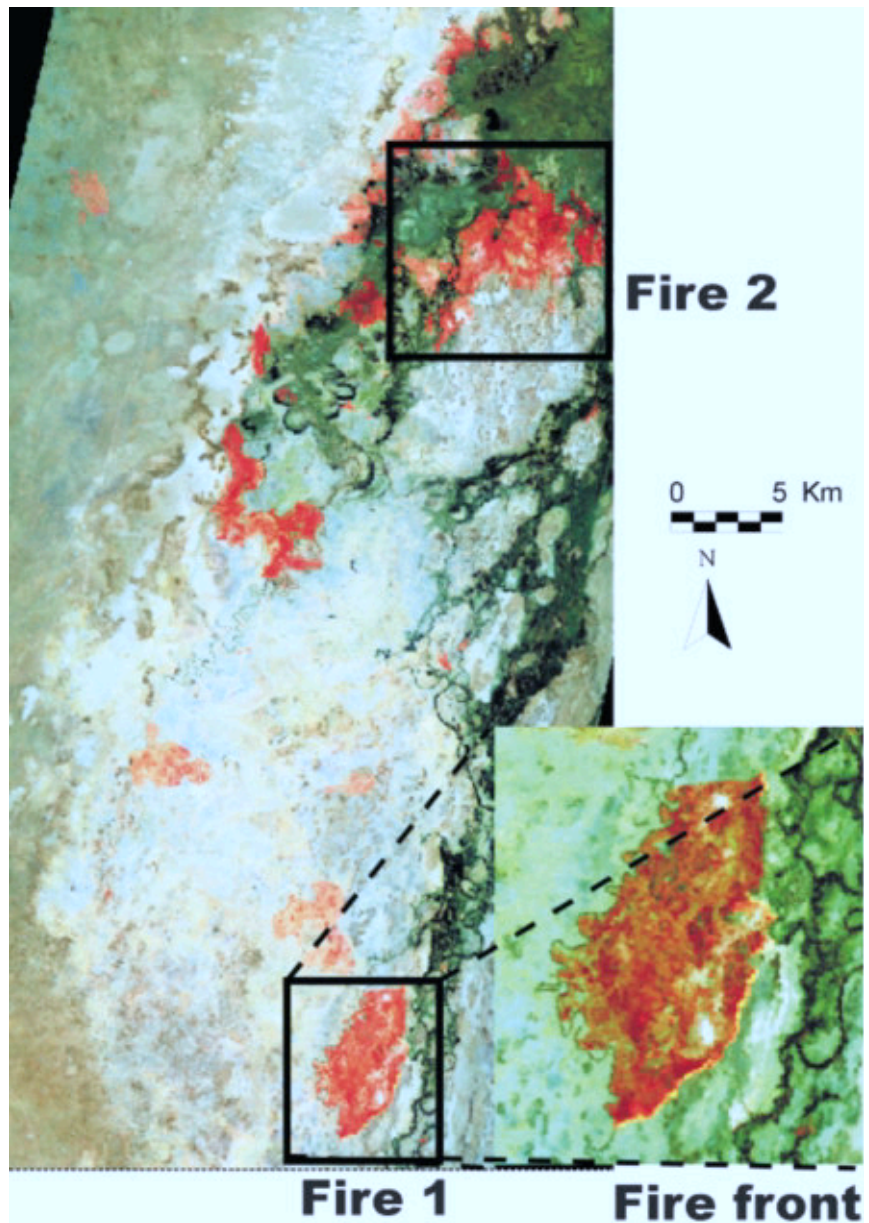


Fig. 7. Peat fires around the Thaoge channel of the Okavango Delta, as registered by the MODIS Airborne Simulator on 27 August 2000. The image area is shown in Fig. 1. Colour composite: blue = 0.66- μm band, red = 1.64- μm band, green = 4.07- μm band (3.28- μm band in fire front detail).

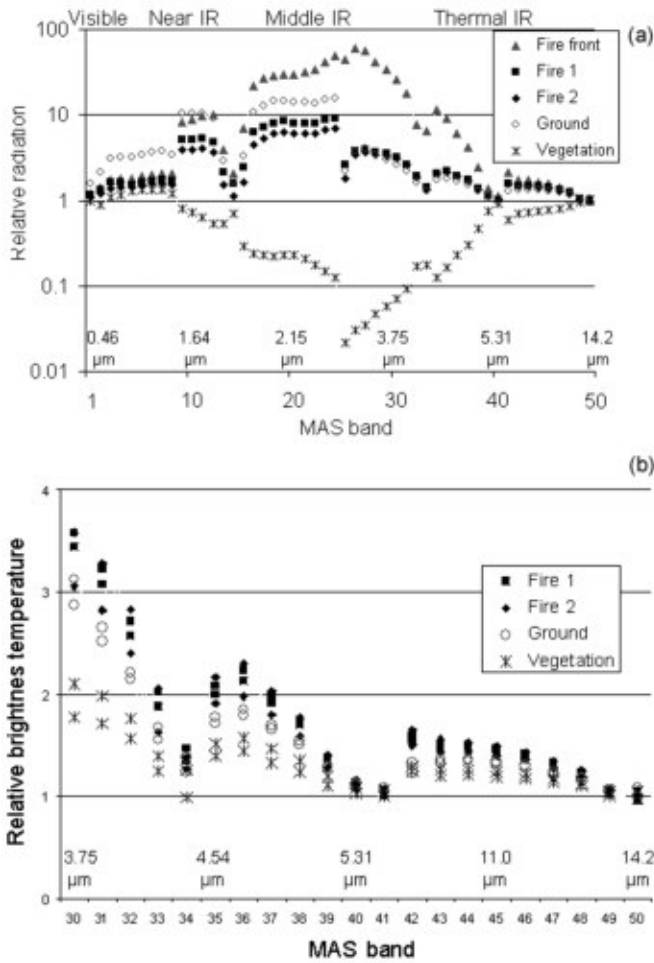


Fig. 8. Diagram of MAS relative radiometric signals from fire front, fires, bare ground and vegetation (see Fig. 3) in the Okavango Delta. The signals are given as related to water (darkest pixel). (a) Logarithmic diagram showing all MAS bands. Note that the bare soil surface has a higher brightness temperature than the smouldering fires below 3.7 μm. (b) Fire detection region showing ± 1 standard deviation for the different types of surfaces. The fires have a significantly elevated radiometric signal except for the 4.4-μm and 5.4-μm bands.

and ATSR data acquired during the day are often saturated in the thermal region during the hot dry season, and application for fire detection requires the inclusion of visible to near-infrared data to discriminate bright soil surfaces, hence allowing for lower brightness temperatures to be identified as fires. The superior MODIS sensor, with relatively high spatial and spectral resolution, holds promise for the detection of sub-surface fires. Separating sub-surface peat fires from low-intensity smouldering surface fires, or from the burn scars of surface fires, requires the adoption of either multi-temporal data for identifying recurring fires or contextual classification confining potential peat fires to former wetland areas juxtapositioned between existing wetlands and peat fire scars.

This study was part of the SAFARI 2000 Southern African Regional Science Initiative. We acknowledge Michael D. King at NASA Goddard Space Flight Center and Jeff Myers at NASA Ames Research Center for MAS science and instrument support, and Harold Annegarn of the University of the Witwatersrand as coordinator of SAFARI 2000. The Swedish Foundation for International Cooperation in Research and Higher Education (STINT) financed scholarships for T.G. and J.M. Infrastructural support was given by the School of Geosciences at the University of the Witwatersrand.

Received 20 November 2001. Accepted 4 July 2002.

1. Ellery WN., Ellery K., McCarthy TS., Cairncross B. and Oelofse R. (1989). A peat fire in the Okavango Delta, Botswana, and its importance as an ecosystem process. *Afr. J. Ecol.* 27, 7–21.
2. Stigand A.G. (1923). Ngamiland. *The Geographical Journal* 62(6), 401–419.
3. Roy D.P., Lewis P.E. and Justice C.O. (in press). Burned area mapping using multi-temporal moderate spatial resolution data — a bi-directional reflectance model-based expectation approach. *MODIS Land special issue of Remote Sensing of Environment*.
4. Swap R.J., Annegarn H.J. and Otter L. (2002). Southern African Regional Science Initiative (SAFARI 2000): summary of the science plan. *S. Afr. J. Sci.* 98, 119–124.
5. Swap R.J. et al. (2002). The Southern African Regional Science Initiative (SAFARI 2000): overview of the dry season field campaign. *S. Afr. J. Sci.* 98, 125–130.
6. Matson M. and Dozier J. (1981). Identification of subresolution high temperature sources using a thermal IR sensor. *Photogram. Engnr Remote Sens.* 47, 1311–1318.
7. Kaufman Y.J., Setzer A, Justice C., Tucker C.J., Pereira M.C. and Fung I. (1990). Remote sensing of biomass burning in the tropics. In *Fire in the Tropical Biota*, ed. J.G. Goldammer, pp. 371–399. Springer, Berlin.
8. Justice C.O., Malingreau J-P. and Setzer A.W. (1992). Satellite remote sensing of fires: potentials and limitations. In *Fire in the Environment*, eds P.J. Crutzen and J.G. Goldammer, pp. 75–88. John Wiley, Chichester.

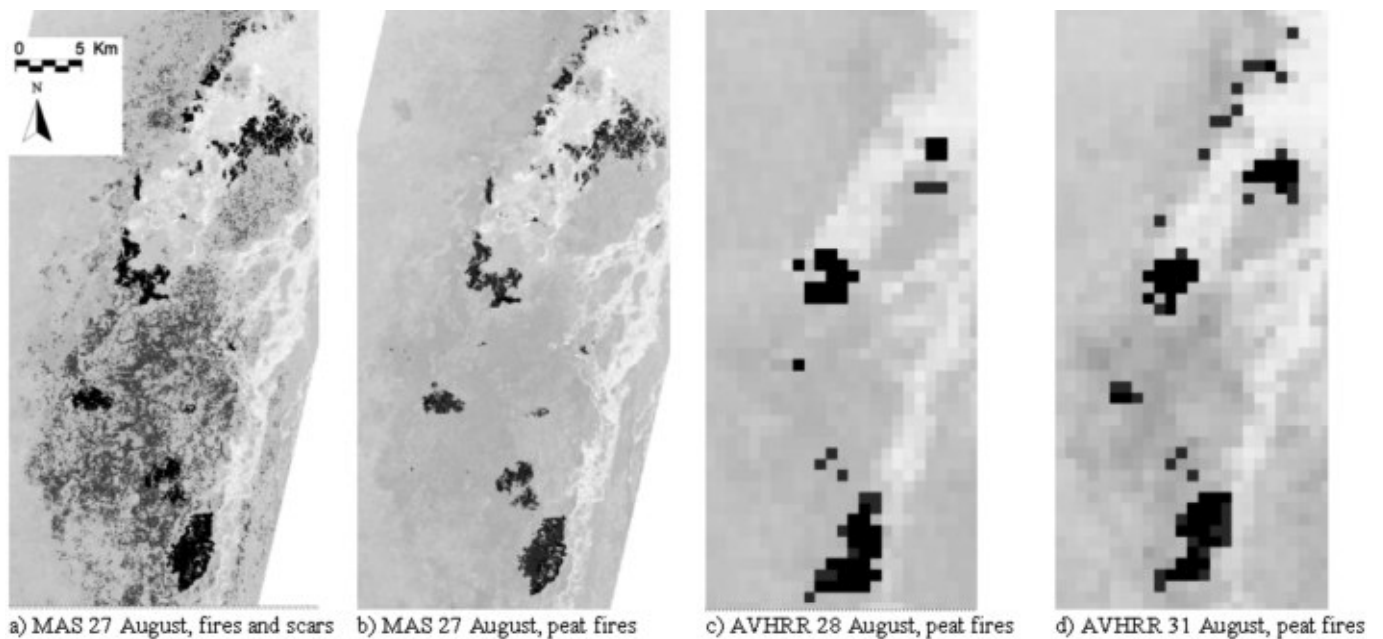


Fig. 9. Peat fires (dark spots) around the Thaoge channel, Okavango Delta, during late August 2000, detected by the MODIS Airborne Simulator and AVHRR sensors. Image backdrop from MAS and AVHRR bands at 3.7 μm. The image area is shown in Fig. 1.

9. Giglio L., Kendall D. and Justice C.O. (1999). Evaluation of global fire detection algorithms using simulated AVHRR infrared data. *Int. J. Remote Sens.* **20**, 1947–1985.
10. Kennedy P.J., Belward A. and Grègoire J-M. (1994). An improved approach to fire monitoring in West Africa using AVHRR data. *Int. J. Remote Sens.* **15**, 2235–2255.
11. Langaas S. (1992). Temporal and spatial distribution of savanna fires in Senegal and the Gambia, West Africa, 1989–90, derived from multi-temporal AVHRR night images. *Int. J. Wildland Fire* **2**, 21–36.
12. Flasse S.P. and Ceccato P. (1996). A contextual algorithm for AVHRR fire detection. *Int. J. Remote Sens.* **17**, 419–424.
13. Pereira, J.M.C., Chuvieco, E., Beaudoin, A. and Desbois, N. (1997). Remote sensing of burned areas: a review. In A review of remote sensing methods for the study of large wildland fires, In *Report of the Megafires Project ENV-CT96-0256*, ed. E. Chuvieco, pp. 127–183. Universidad de Alcalá, Alcalá de Henares, Spain.
14. Roy, D.P., Giglio, L., Kendall, J.D. and Justice, C.O. (1999). Multitemporal active-fire based burn scar detection algorithm. *Int. J. Remote Sens.* **20**, 1031–1038.
15. Fraser, R.H., Li, Z. and Cihlar, J. (2000). Hotspot and NDVI differencing synergy (HANDS): a new technique for burned area mapping over boreal forest. *Remote Sensing of Environment* **74**, 362–376.
16. Arino O. and Rosaz J. (1999). 1997 and 1998 World ATSR Fire Atlas using ERS-2 ATSR-2 Data. *Proceedings of the Joint Fire Science Conference*, Boise, 15–17 June 1999, Volume 1, pp. 177–182.
17. Eva, H. and Lambin E.F. (1998). Burnt area mapping in Central Africa using ATSR data. *Int. J. Remote Sens.* **19**, 3473–3497.
18. Kaufman Y.J., Justice C.O., Flynn L.P., Kendall J.D., Prins E. M., Giglio L., Ward D.E., Menzel W.P. and Setzer A.W. (1998). Potential global fire monitoring from EOS-MODIS. *J. Geophys. Res.* **103**, 32215–32238.
19. Vermote E.F., El Saleous N.Z. and Justice C.O. (in press). Operational atmospheric correction of the MODIS data in the visible to middle infrared: first results. MODIS Land special issue of *Remote Sensing of Environment*.
20. Koutsias N. and Kartertis M. (1998). Logistic regression modelling of multi-temporal thematic mapper data for burned area mapping. *Int. J. Remote Sens.* **19**, 3499–3514.
21. Chuvieco E. (1999). Measuring changes in landscape pattern from satellite images: short-term effects of fire on spatial diversity. *Int. J. Remote Sens.* **20**, 2331–2346.
22. Brustet J.M., Vickos J.B., Fontan J., Podaire A. and Lavenau F. (1991). Characterization of active fires in west African savannas by analysis of satellite data: Landsat thematic mapper. In *Global Biomass Burning*, ed. J.S. Levine, pp. 53–60. MIT Press, Cambridge, MA.
23. Rao C.R.N. and Chen J. (1999). Revised post-launch calibration of the visible and near-infrared channels of the Advanced High Resolution Radiometer (AVHRR) on the NOAA014 spacecraft. *Int. J. Remote Sens.* **20**, 3485–3491.
24. Bartoliucci L.A. and Chang M. (1988). Look-up tables to convert Landsat TM thermal IR data to water surface temperatures. *Geocarto Int.* **3**, 61–67.
25. Van de Griend A.A. and Owe W. (1993). On the relationship between emissivity and the normalized difference vegetation index for natural surfaces. *Int. J. Remote Sens.* **14**, 1119–1131.
26. Miura T., Huete A.R., van Leeuwen W.J.D and Didan K. (1998). Vegetation detection through smoke filled AVIRIS images: an assessment using MODIS band passes. *J. Geophys. Res.* **103** (D24), 32001–32011.